Journal of Engineering, Science and Technology
ISSN: 2714-2396, Volume 8 Issue 1

TRANSVERSE DISPERSION OF DYE PLUMES IN COASTAL MEDIA USING THE SPATIAL SEGMENTATION AND CONTOUR MODELS

Okuroghoboye Diepreye Itugha[1]

[1]Faculty of Engineering, Department of Civil Engineering, Federal University Otuoke, PMB 126, Bayelsa State, Nigeria.
Email: diepitu@yahoo.com

Received Date: 23 July 2024 Accepted Date: 30 April 2025 Published Date: 4 June 2025

ABSTRACT: This paper evaluates transverse advective dispersion of dye plumes recovered in coastal subsurface media using spatial segmentation and contour analyses. The results of the analyses suggest that dispersion can be associated to contaminants, nutrients and organic matter fluxes at the sediment-seawater interface. A pore-water transport scheme was designed and demonstrated in-situ by injecting prescribed volumes of dye solution into porous coastal sand beach during ebb-tide. The reaction of the dye due to semi-diurnal dynamics of tides was monitored over time not exceeding seven days. Several distinctive features of dye plumes (full three dimensional cross-sections) was captured in situ at the injection points. The recovered plume samples differ from previous contaminant monitoring tests in aquifers, such as spherical/elliptical shapes as reported in literature. The plumes here showed significantly large spatial variability, diverging upwards and converging downwards, with conical geometric shapes. Spatial segmentation, calibration and concentration information of the plumes were estimated to enable the interpretation of the dispersed dye in the porous media. A Gaussian model in matlab was applied on the calibrated plume data to simulate the contours of concentration curves described in the data points. The coefficient of apparent dispersion obtained from the results was not constant as shown in the transverse concentration curves. The transverse concentration output suggest symmetry showing clearly that within the surficial subsurface region some uniformity of sorts is being described. This characteristic profile however, was not sustained long at the peak of concentration but drops fairly rapidly approaching zero within the sampling time frame. This implies that relative anisotropic variations could influence increase in the distribution of concentration. Dispersion is therefore affected due to broader effects of the velocity regimes attributable to combinations of intertidal and other environmental consequences.

.

Keywords: *Coastal dynamics, dye plume, advective dispersion, interstitial hydraulics, spatial segmentation.*

1. INTRODUCTION

In the words of Ford and Williams (1989) “water tracing is a well-developed powerful tool of the karst hydrologist, enabling catchment boundaries to be delimited, groundwater flow velocities to be estimated, areas of recharge to be determined and sources of pollution to be identified”. Dye experiments enable the assessment of the depth of advective solute exchange in beach sands (Boudreau et al, 2001; Itugha et al, 2016). In the crude-oil-rich Niger Delta region of Nigeria, surficial inland - offshore tides have been found to induce large fluxes exceeding interstitial diffusive flux in the beach vadose zone (Boufadel et al. (2006); Itugha et al, 2016)) from post spill impact assessment (PSIA) studies, especially in the widely publicized November - December 2021 Santa Barbara Well-1 oil/gas blowout incident.

Model methods for hydraulic gradients and conductivity towards understanding surface-ground water interactions have been cited severally. Especially, the effects of fluid parcels undergoing transport in macro-pore regions, ranging from Hazen's grain size to application of piezometers. The continued interest by researchers to this study implies increased demand of relational knowledge that is necessary between the hyporheic zone and the ecology of natural habitats (Boulton et al, 1998). Tillmann et al (2008) used estimated grain size distribution data obtained from a cone penetration test (CPT) survey to calculate hydraulic conductivity values for a subsurface flow field in Krauthausen, Germany. Another research work by Kløve et al (2005) represented the vadose zone to a filter by conducting measurements of hydraulic conductivity using what they called subsurface flow filters (SSF) using tracer tests. Precht and Huettel (2004) measured pore water velocities in the field using optode techniques with a view to studying interactions between the groundwater flow field and surface water, but could not obtain quantitative data of the injectate concentrations in their study area due to poor signal output. Baxter et al (2003) also proposed a new technique by installing mini-piezometers which enabled them to give estimates of vertical hydraulic gradients for hydraulic conductivity, and pore-water velocities.

The present study applied visual scaling technique (VST) using response plumes of injectate solutes in the subsurface (Itugha, 2008). Apart from the rigors of field excitement, the VST is a relatively similar application of Darcy's falling-head and Hvorslev's methods. The method offers the investigator the ability to access the reality of the developing plumes in their true nature within the subsurface undisturbed and measure the response outcome physically. This forecloses the use of complex mechanisms like the use of some optical probes or sensors, so that the objectives of obtaining representative quantitative and qualitative records including pore-water velocities are not misplaced. The scaling method in the present study was done during the lowest low tides (low ebbs) when the foreshore is free of flood water. That is, when the streamline is furthest from the shoreline. The digital images of the plumes were enhanced and colour calibrated to optical density values (Itugha et al, 2016, 2020). Interstitial hydraulic studies of this nature are essential as the procedure captures the effectiveness of tracer test to simulate the fate and transport of underlying contaminants in transit and so the mapping of groundwater flow fields. This can enhance practice-based research (PBR) as well as for post-doctoral research studies.

2 STUDY AREA, EXPERIMENTAL DESIGN AND METHOD

The study area has large cross-sections of industrial presence with increased catchment population, both affect scales of freshwater pumping and utility which are water quality management issues. The location of the site, experimental design and methods has been discussed fully in Itugha et al, 2016.

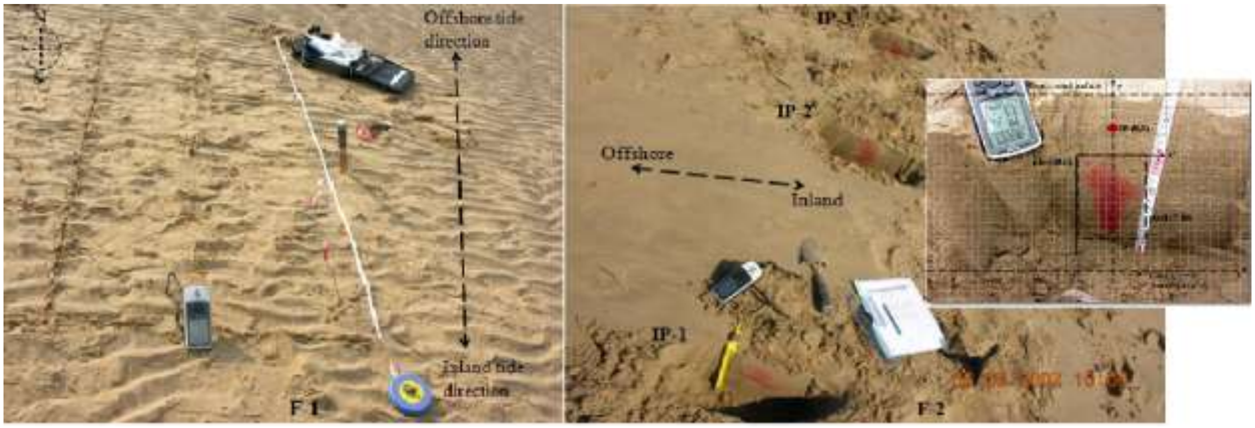

Fig 1: Arrangement of rectangular cross-section of injection position (IP) surveying and mapping for injection in VST in a typical field site with column/row divisions on the foreshore; F-1 (Rectangular arrangement on field), F-2 [Excavated column of IPs with cross-section showing area-of-interest (AOI), x′,y′ in thickly-doted rectangular lines relative to the point of reference (injection depth) above it].

The method approximately simplifies to mounting calculated volumes (5.0ml) of injectate solute into injection depth (ID) of 0.05m by the aid of hypodermic/luer needles using purge and trap syringe (10.0ml). Each portion was injected into marked geometries of rectangular arrays composed of 0.5m x 0.5m square cells on the coastal foreshore. The respective locations of the IPs were identified with a 12 channel Garmin GPS 76 marine navigator, which also acts as a guide instrument and location mapper, correct to about 1-2m precision. The experiments were specifically monitored through temporal durations of semidiurnal tides that load the coastal foreshores (Itugha, 2008). At the end of each monitoring session, the events were excavated carefully to penetrate the plume domains undisturbed, measured and the images photographed as earlier described (Fig 1). This was succeeded by data processing and analyses.

2.1 QUANTIFICATION OF PLUME IMAGES AND ANALYSIS

The contaminated surface area (l x b) at each IP was recovered, carefully sectioned or penetrated and the undisturbed plume domain photographed. The volume (l x b x h) of the plume domain was sliced from the edge towards the center of the square (l x b) in each case to maximize recovery and measurement of the plume shape fully (Fig. 1). A graphical analysis of the plume with coordinates using a trapezoidal identity showing parameterization of the vertical extent, depth of plume center and the top and bottom widths at various elapse times have been discussed extensively (Itugha et al, 2016; 2020). A Cartesian coordinate system was established using the horizontal line passing the injection point as the x-axis and a vertical line some distance away from the plume center line as the y-axis.

2.2 PREPROCESSING OF COLOR IMAGES

Each of the photographic colour images represents a variation of three primary colour components red, green and blue (RGB) or known as image true colour. The use of image pro-plus (IPP) enables the identity of each pixel of RGB image as consisting equal-bit value and supports up to 48-bit colour images. Emphasis in this case is on relating the intensity (I) values associated with these colors to the simulate chemical concentration. Intensity (I) can result from the mean value of the three colour components [$I = (R + G + B)/3$] scaled as gray level. According to Lambert-Bear's law, $I_r = 1.0E(-\varepsilon Cl)$, where $I_r = I/I_0$ = relative intensity, I = light intensity leaving the target image, I_0 = light intensity striking the target image, C = concentration of the simulate chemical, l = length describing path taken by light, and ε = molar absorptivity (extinction coefficient). In this study however, the relation between the color intensity of the images and color concentration of the solute chemical was determined by the method of calibration and setting thresholds (0 or 1) to each color pixels. Firstly, the spatial distribution of color intensities was standardized to optical density intensity data and converted to concentration profiles using a least square relationship. Schincariol et al. (1993) and McNeil et al. (2006) emphasized the standardization of image color intensities to optical density (ρ_{opt}) levels.

The intensity scales of image plumes in the process was calibrated and expressed as standard optical density data. The conversion to optical density was done through the 'measure' submenu by calling the intensity command after successful spatial calibration. The command activates the intensity calibration window and the standard optical density option was checked in favour of the gray scale. The emergent exponential curve interprets the optical density scale as inversely related to the optical density data $\left[\rho_{opt} = \log_{10}(m/I)\right]$, where ρ_{opt} = optical density intensity and '*m*' implies constant of proportionality. The ratio of optical density/intensity reflects that larger intensities would mean lesser optical density values. The standard deviations of the colour patches were evaluated in 2-D space with time across the entire cross-section of the segmented plume: $\sigma_x(t) = \left(N^{-1}\sum\left(x - \bar{x}_c(t)\right)^2 . f(x,y,t)\right)^{0.5}$ and $\sigma_y(t) = \left(N^{-1}\sum\left(y - \bar{y}_c(t)\right)^2 . f(x,y,t)\right)^{0.5}$. Where $\bar{x}_c(t)$ and $\bar{y}_c(t)$ represent the average spatial increments of the plume cross-sections.

Individual calibration of the transverse and longitudinal dispersion of the plumes was done, where the Gaussian Operator in Matlab $C(x) = ae^{\left[-((x-b)/\sigma)^2\right]}$ was applied, where $D = \sigma^2/4t$ = dispersion, σ = peak plume size or mixing length/width, b = peak location of center of plume and $a = \left(\sqrt{4\pi Dt}\right)^{-1}$ = peak amplitude (Itugha et al, 2020).

3.0 RESULTS AND ANALYSIS

3.1 Determination of transverse dispersion coefficient (Variations in transverse transport from Day-1 to Day-5)

The fitted results shown in Figures (2 – 9) are typical shapes and trends of the plumes analyzed from the sites. The plot in Fig 2 represents transverse cross-section of the plumes analyzed from one of the sampling points (OEIS-IZ (A)) (Itugha et al, 2016) for an average time of 25.81±0.40hrs (Day-1).

Figs 2 and 3 show Gaussian shapes in 2D and also in 3D form of 'bi-harmonic' surfaces interpolation respectively. The assumed constant velocity derived from the zone is 0.003475m/hr which can be applied with the individually calibrated apparent dispersion coefficient [D = $\sigma^2/(4t)$] to simulate the concentration distribution information for this plume (Table 1). The result was compared to the effective transverse dispersion coefficient derived from the slope method [D = $1/(4m_x t)$] (Table 1). The fit is good with correlation coefficient (R^2) percentage of 93.61 and bell-shape describing Gaussian features relative to the centroid. The SSE and RMSE of this figure are small, 0.00217 and 0.00639 respectively (Table 1). The 3D Gaussian bi-harmonic interpolation is computed from the coefficient structure where *x* and *y* are normalized by the means 0.0275 and 0.0216 with the standard deviation 0.0163 and 0.00163 respectively. The variation of concentration (color bar) is described in the bi-harmonic surface as symmetry of the Gaussian profile. The symmetric behaviour of the concentration distribution can also be demonstrated in terms of contours (Fig 4). The contours complement the resulting data showing the concentration front of the plume to increase to its peak at the position (2.5, 2.12) cm from the centre before it decreases approaching zero.

The transverse concentration output show symmetry compared to the asymmetrically left-skewed longitudinal concentration curve obtained in the vertical (Itugha et al, 2020). Clearly within the surficial subsurface region some uniformity of sorts is described by the transverse concentration profiles. This characteristic profile however, was not sustained long at the peak of concentration but drops fairly rapidly approaching zero within the sampling time frame. The transport variables (dispersion and average velocity) were found within 95% confidence intervals (Itugha, 2008). This behavior may imply that, relative anisotropic variations could influence increase in the distribution of concentration as dispersion is affected due to broader effects of the velocity regimes (Li and Ghodrati, 1995).

The fits on Day-2 also show good correlation between experiment and theory (Fig 5). The data points describe the observed concentration trend in a bell-shape describing Gaussian profiles. The Gaussian operator minimized the experimentation errors through the solid-line that relate the trend of the symmetric concentration path. The effective dispersion coefficient value for the transverse cross-section of this particular plume and goodness-of-fit estimates between model and observed are given in Table (1).

The shape of transverse distribution model on Day-3 also fitted the experimental data well in Fig 6. The average area of the shapes of plumes increased compared to Days-1/-2. The Gaussian operator shows a smooth peak defining symmetric outline of the distribution by minimizing obvious errors between the observed data and model. The calibrated apparent dispersion coefficient increased compared to Days-1/-2 (Table 1).

The movement transverse to the flow in Fig 7 represents a full 2-D plume for Day-4 which predicts the behaviour of concentration transport in the subsurface. The model fitted the experiment data well, implying that the curve is symmetric and identify with Gaussian distribution. The calibrated dispersion coefficient in this case slightly reduced which also affected the peak width of the plume. The point could be made that the development of the full plume in the subsurface may be partly dependent on the behaviour of both transverse and longitudinal pathways. It is possible therefore that continuous increase in the longitudinal flow direction can impact on consistency in the development of transverse cross-section of the plume. The goodness-of-fit (SSE, R-square, RMSE) and dispersion values for this case can be found in Table (1) showing relatively small errors with significantly high correlation coefficient (R^2) value.

Fig 8 shows the concentration distribution information for the transverse cross-section of the Day-5 plume. The concentration pathline of the plume give a general understanding to the nature of contaminant pathways up to Day-5. The best-fit pathline fitted the observed data well minimizing obvious errors between experiment and model-fit. The goodness-of-fit estimates show relatively small errors with significantly high correlation coefficient (R^2) value. The concentration distribution in the transverse direction reflects a Gaussian profile and symmetric suggesting uniformly packed beach-sand in the transverse cross-sections of the near-surface zones. The calibrated apparent dispersion coefficient for this fit can be found in Table (1) with error comparisons, showing that the model fitted the data points well.

A comparison of the variations of concentration distribution due to the dynamic impact of the tides on the injectate for the transverse plane from Day-1 to Day-5 is shown in Fig 9. The fit between experiment and model correlates well. There is a clear difference in the movement of plumes from Day-1 to Day-5 giving rise to relative increase in the peak widths as dispersion was also found to increase. The individually calibrated apparent dispersion coefficient [$D = \sigma^2/(4t)$] varied such that on Day-1 it was lowest with $9.3424\text{x}10^{-05}\text{m}^2/\text{hr}$. On Day-2 the dispersion coefficient was $1.2819\text{x}10^{-04}\text{m}^2/\text{hr}$, on Day-3 it was $1.6516\text{x}10^{-04}\text{m}^2/\text{hr}$, Day-4 estimate was $1.7658\text{x}10^{-04}\text{m}^2/\text{hr}$ and the estimate of dispersion coefficient for Day-5 was $1.8197\ \text{x}10^{-04}\text{m}^2/\text{hr}$, with relatively increasing plume displacement width at increasing time-distance ratios. The results assume the transverse dispersion coefficient as a linear function of the growth in the injectate pool from the point of injection.

Table 1: Transverse [D_{hT} (m^2/hr)] dispersion coefficients obtained using the Gaussian operator[2], with values from the slope or simultaneous technique.

Time (hr)	σ (m)	Gaussian D_{hT} (m^2/hr)	Slope D_{hT} (m^2/hr)	SSE	R-square	RMSE
25.81±0.40	0.01015	2.0911E-05	4.6873E-05	0.002165	0.9361	0.006392
49.82±0.25	0.008114	2.303E-05	2.171E-04	4.546E-03	0.9772	0.009441
74.94±0.36	0.01419	3.555E-05	1.208E-04	2.11E-05	0.9719	0.000527
98.83±0.49	0.008766	2.972E-05	5.153E-05	9.055E-04	0.9664	0.003761
125.12±0.69	0.01436	2.875E-05	2.585E-04	0.01713	0.8806	0.01611

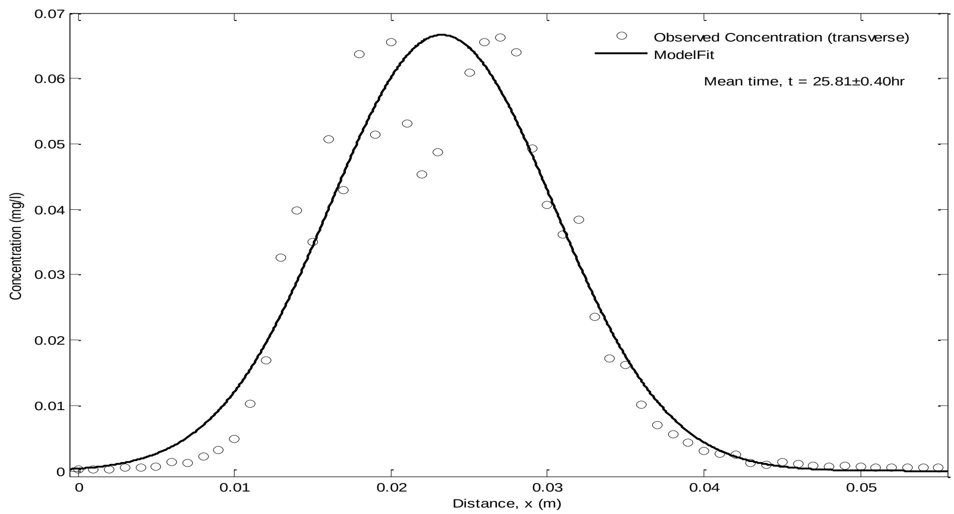

Fig 2: Day-1 2D 'Gaussian' model showing symmetric behaviour of the transport of injectate concentration in the sediments as a function of distance under natural oscillatory tides, along flow transverse to the vertical plane.

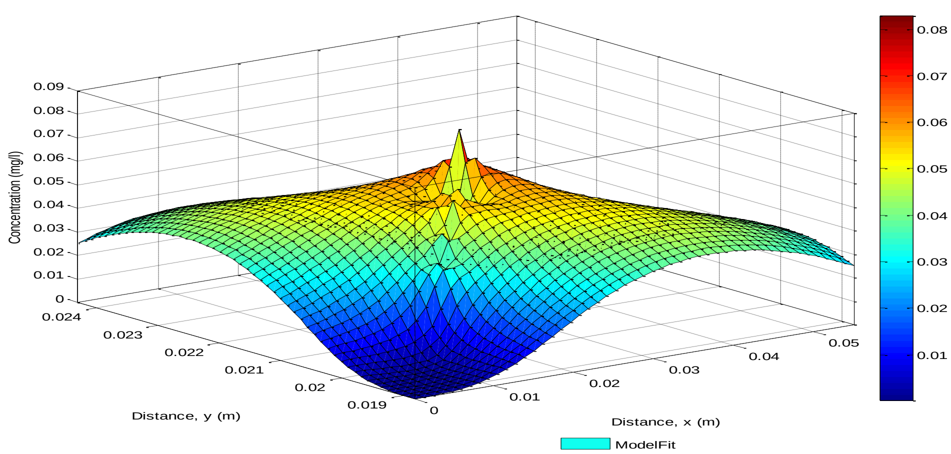

Fig 3: 3D spatial description of the concentration (transverse), using bi-harmonic interpolation along x and y. The color-bars show the variation of concentration transverse to the vertical dimension.

[2] In **Table 1**, the Gaussian model describe the concentration $C(x) = ae^{\left[-((x-b)/\sigma)^2\right]}$; where a = peak amplitude, b = peak location of plume center, σ = peak width of plume distribution; $D = \sigma^2/4t$ =apparent dispersion; and the slope method $D_x = (4m_x t)^{-1}$, and $D_y = (4m_y t)^{-1}$ where m_x = transverse slope, m_y = longitudinal slope. SSE = sum of squared errors, RMSE = root mean square error.

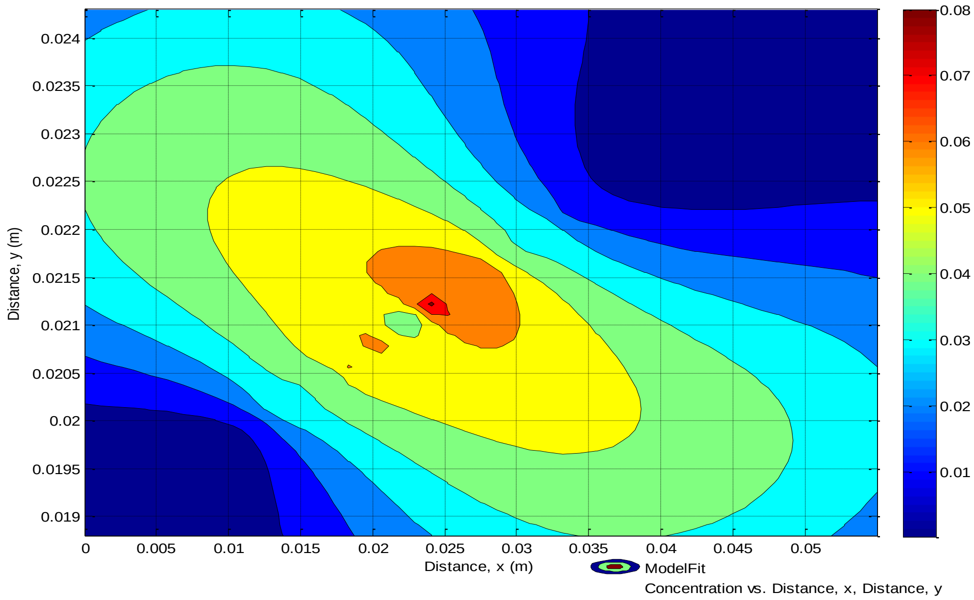

Fig 4: Spatial description of the concentration (transverse), using contours along x and y. The color-bars show the variation of concentration transverse to the vertical plane.

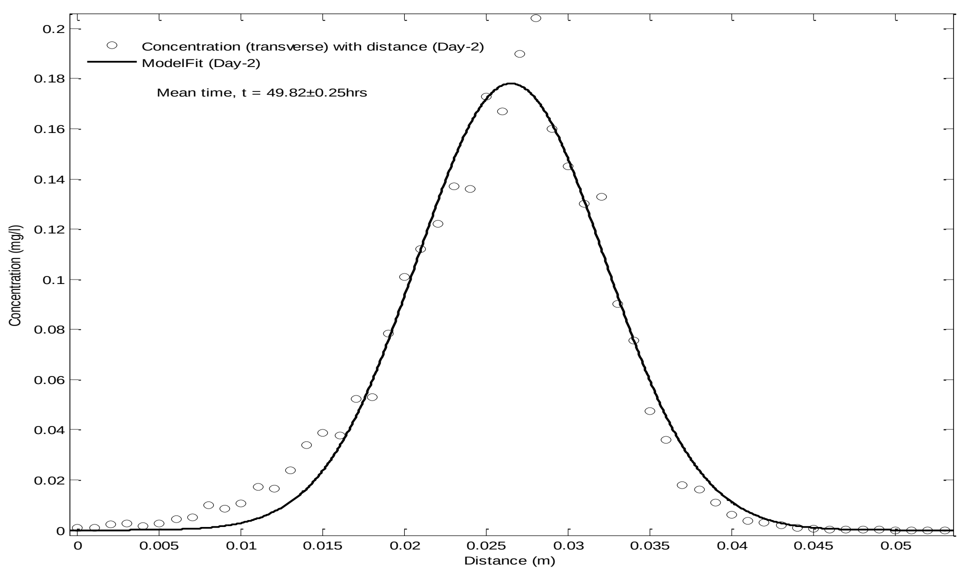

Fig 5: Day-2 2D 'Gaussian' model showing symmetric behaviour of the transport (transverse) of injectate concentration in the sediments as a function of time under natural oscillatory tides. Solid line indicates the 'Gaussian' fit.

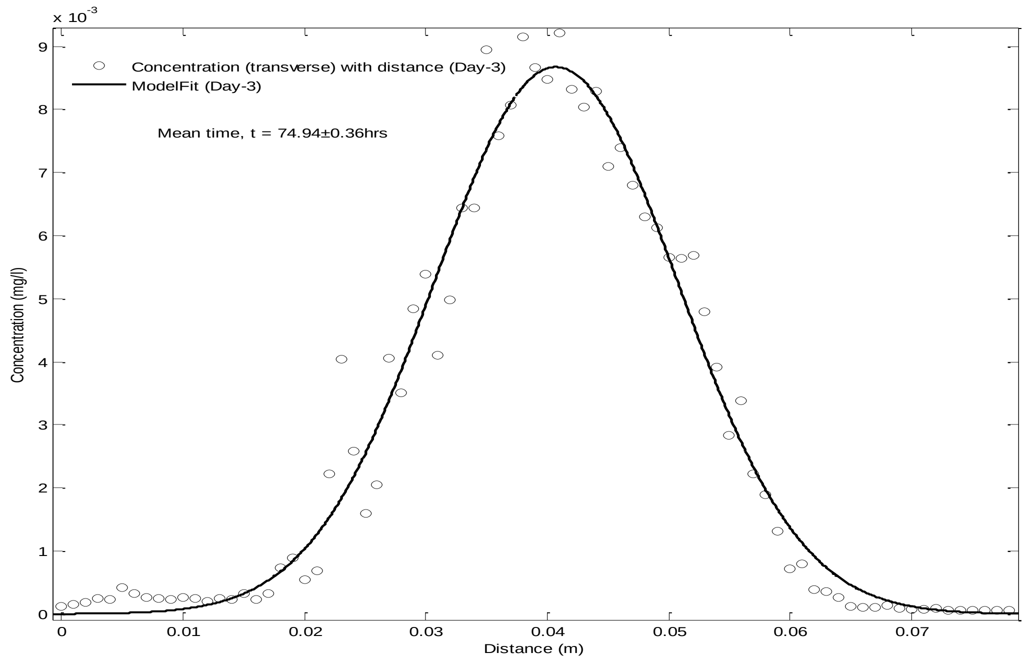

Fig 6: Day-3 2D 'Gaussian' model showing symmetric behaviour of the transport (transverse) of injectate concentration in the sediments as a function of time under oscillatory tides.

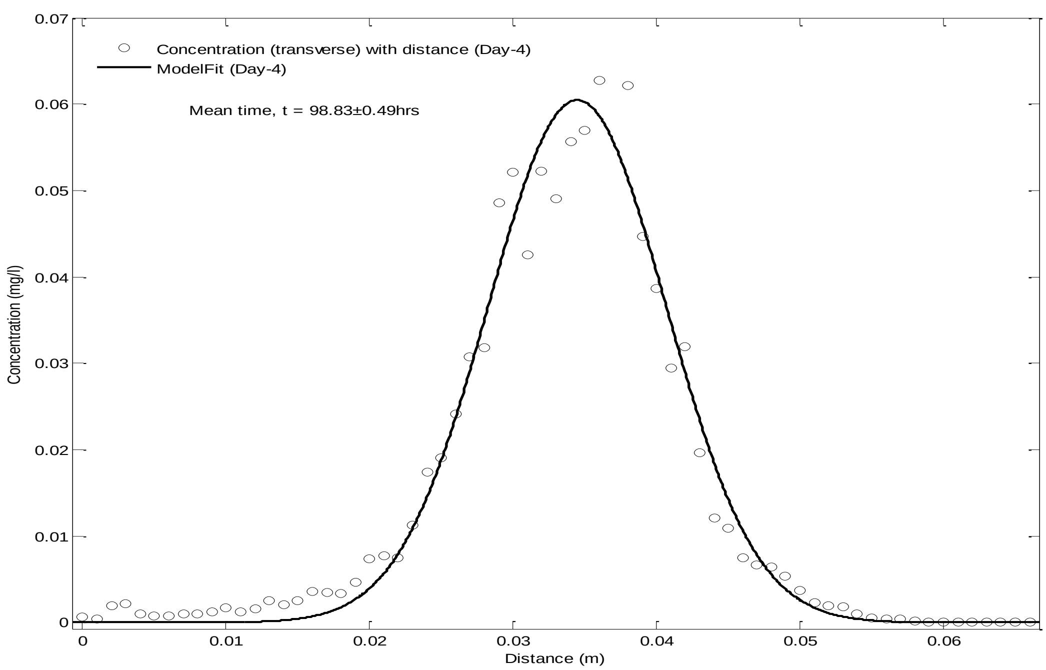

Fig 7: Day-4 2D 'Gaussian' model showing symmetric behaviour of the transport (transverse) of injectate concentration in the sediments under oscillatory tides.

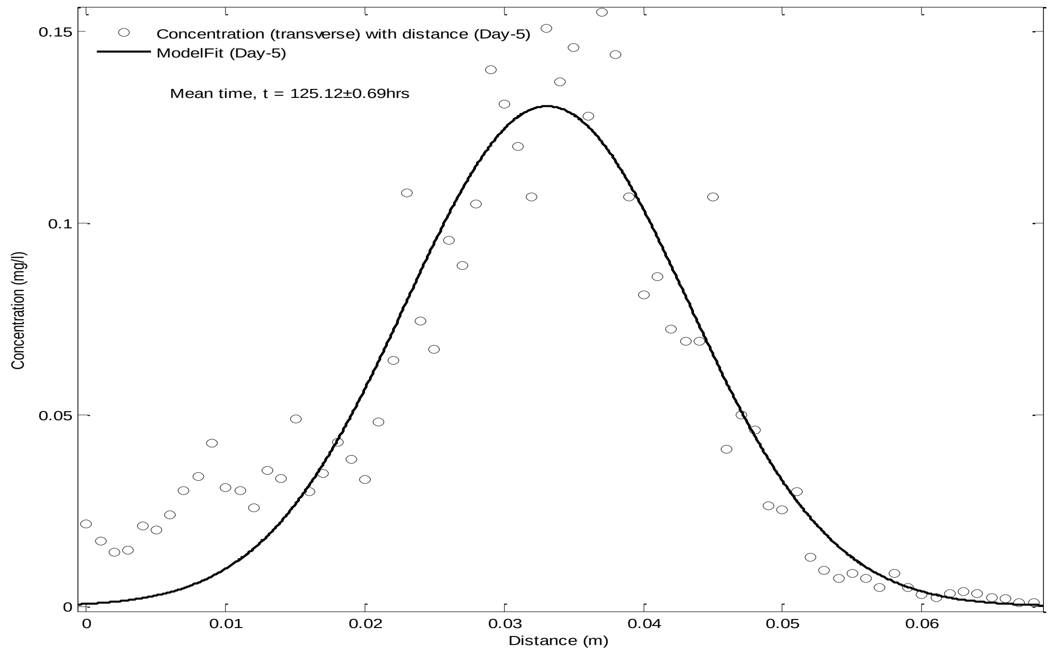

Fig 8: Day-5 2D 'Gaussian' model showing symmetric behaviour of the transport (transverse) of injectate concentration in the sediments with time under natural oscillatory tides.

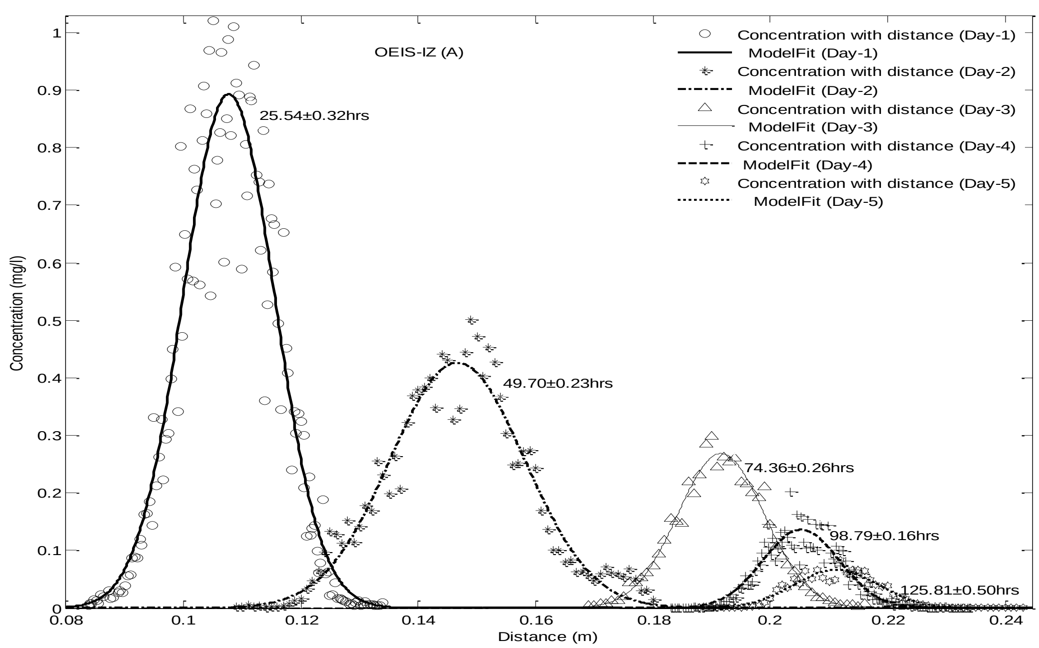

Fig 9: Comparison of observed and fitted concentrations with distance over time for convergent tracer experiments in the summer for Day-1 to Day-5 at the OEIS-IZ (A) site.

4.0 CONCLUSION

The research is a product of experiments involving non-invasive technique (Robbins 1989), the IPP in addition to Matlab scripts have been successfully applied to process colour images of dye plumes recovered in subsurface foreshores, as required in non-invasive techniques (Robbins 1989). Thus conventional techniques are incorporated to enhance clarity in this unique problem of solute movement and transport in coastal sediments which is different to solute transport in groundwater aquifers.

A Gaussian model in matlab was applied on calibrated plume data to simulate the contours of concentration curves described in the data points. It enabled the interpretation of the patterns of observed plume images recovered from the field so that we have results of the dispersive parameters associated to the distribution of the chemical. The effective dispersion coefficient estimates determined simultaneously (Chen et al 1999), using slopes derived from the advective dispersion equation (ADE), were compared to the individually calibrated results using the Gaussian operator in Matlab. Descriptions of these data for all experimentation zones with 95% confidence intervals are shown in Table (1). The results show that coefficient of apparent dispersion was not constant as shown in the transverse concentration curves. I believe the non-uniformity may be associated to the varying phenomenon of mechanical processes affecting flow in the subsurface as indicated in the concentration curves from the plumes. The erratic patterns observed in the concentration curves were relatively particular to early times in the experiments after solute injection especially in the longitudinal flow of winter season (Itugha, 2008). Also, the patterns of plume response may not be attributable to singular but combinations of environmental consequences. The uniqueness of the findings may therefore need further investigations or clarifications particularly the influence due to permeability, the semi-diurnal tides and the role of salinity using numerical methods.

However, it is reasonable to suggest that the surface water (SW) and groundwater (GW) connected to the vadose zone of the study field are vulnerable to diffuse contaminants. The individually calibrated profiles of the plumes show that the surficial zones of the study area are relatively uniform (homogeneous and isotropic) from the predominantly symmetric concentration curves encountered in the lateral (offshore-inland) directions of flow. This is in agreement with the laboratory data except for the vertical directions of flow where the concentration curves deviate in the field results to describe unique patterns of asymmetry or non-Gaussian trends. I have associated the asymmetry here to relative inhomogeneity and anisotropy of the beach-sand in the vertical terrain (lower depths) approaching the vicinity of the water table. It shows the characteristics associated to mediums reflecting similar properties such as decreasing hydraulic conductivity, increasing dispersion and concentrations. In-spite of the 2D Gaussian models applied to data, I have also reflected the behaviuor of the plumes using bi-harmonic surface interpolations and contours to describe and portray different aspects of the movement and transport phenomenon.

The study finds the dynamic exchange phenomenon between GW and SW driven by semidiurnal tides synonymous with the study terrain as responsible in causing significant flux activity at the outer River Mersey Estuary (RME) beach. This flux activity has the potential to drive or transport diffuse nutrients and contaminants either into the GW or SW or both simultaneously in the study field.

References

[1] Baxter C, Hauer RF and Woessner WW, 2003. Measuring groundwater-stream water exchange: New techniques for installing minipiezometers and estimating hydraulic conductivity. Transactions of the American Fisheries Society 132:493-502.

[2] Boudreau, B.P., Choi, J., Meysman, Filip, François-Carcaillet, F., 2001. Diffusion in a lattice-automaton model of bioturbation by small deposit-feeders. J. Mar. Res. 59, 749e768.

[3] Boufadel, M.C., Suidan, M.T., Venosa, A.D., 2006. Tracer studies in laboratory beach simulating tidal influences. J. Environ. Eng. 6, 132.

[4] Boulton, A. J., S. Findlay, P. Marmonier, E. Stanley, and H. M. Valett. (1998). The functional significance of the hyporheic zone in streams and rivers. Annual Review of Ecology and Systematics 29:59–81.

[5] Chen, J. S., Chen, C. S., Gau, H. S., Liu, C. W., (1999). A two-well method to evaluate transverse dispersivity for tracer tests in a radially convergent flow field. J. Hydrology; 223 (3-4): 175-97.

[6] Ford, D. and Williams, P. (1989) Karst Geomorphology and Hydrology, Unwin Hyman Ltd, London.

[7] Okuroghoboye D. Itugha, D. Chen, and Y. Guo (2016), Pollutant advective spreading in beach sand exposed to high-energy tides. Estuarine, Coastal and Shelf Science, Vol.181, pp.70-82, http://dx.doi.org/10.1016/j.ecss. 2016. 08.011. 2016 Elsevier Ltd.

[8] Okuroghoboye D. Itugha, Emmanuel E. Jumbo, and Efosa Obaseki (2020). *Determination Of Subsurface Coastal Dispersions Using Dye Plume Contour Simulation And Spatial Segmentation Analysis*. Journal of Multidisciplinary Engineering Science Studies (JMESS). ISSN: 2458-925X. Vol. 6 Issue 1, January – 2020.

[9] Okuroghoboye D. Itugha, 2008. Solute and Particulate Transport at the Interface of Near-shore Permeable Estuarine Beach-sand: An Experimental Study of the Outer Reaches of River Mersey Estuary, N W England. Harold Cohen. THESIS 20860.ITU, Liverpool: Thesis Ph.D., 2008.

[10] Kløve, B., Xu, S., Lindahl, A., Wörman, A. and Søvik, Anne-Kristine (2005). A Study of K Variability and its effect on solute transport in subsurface-flow sand filters by measurement and modelling. Journal of Environmental Science and Health, 40:1123–1132, Taylor & Francis Inc.

[11] Li, Y., Ghodrati, M. (1995). Transport of nitrates in soils as affected by earthworm activities. J. Environ. Qual. 24: 432-438.

[12] McNeil, J. D., Oldenborger, G. A., and Schincariol, R. A. (2006). Quantitative imaging of contaminant distributions in heterogeneous porous media laboratory experiments. J. Contam. Hydrol., 84: 36–54.

[13] Precht, E., Huettel, M. (2004). Rapid wave-driven advective pore water exchange in a permeable coastal sediment. Journal of Sea Research, Vol. 51, pp. 93–107.

[14] Robbins, G. A. (1989). Methods for determining transverse dispersion coefficients of porous-media in laboratory column experiments. Water Resource Research 25:1249–58.

[15] Schincariol, R.A., Herderick, E.E., Schwartz, F.W. (1993). On the application of image analysis to determine concentration distributions in lab expts. J. Contam. Hydrol. 12: 197-215.

[16] Tillmann, A., Englert, A., Nyari, Z., Fejes, I., Vanderborgh, J., Vereecken, H. (2008). Characterization of subsoil heterogeneity, estimation of grain size distribution and hydraulic conductivity at the Krauthausen test site using Cone Penetration Test. Journal of Contaminant Hydrology 95 (2008) 57–75.